Energy materials

CrossMark

N-doped carbon-encapsulated MnO@graphene nanosheet as high-performance anode material for lithium-ion batteries

Tao Bai[1], Haochen Zhou[2], Xiangyang Zhou[1], Qunchao Liao[1], Sanmei Chen[1], and Juan Yang[1,*]

[1] *School of metallurgy and Environment, Central South University, Changsha 410083, China*
[2] *Department of Aerospace, Tsinghua University, Beijing 100084, China*

ABSTRACT

MnO is a promising anode material for lithium-ion batteries because of its high capacity and abundant source, yet some critical issues such as the low conductivity and huge volume changes during cycling are still challenging its real application. Here, a facile strategy is proposed to realize the uniform decoration of MnO nanoparticles (20–40 nm) on graphene encapsulated with N-doped carbon layer (MnO@rGO/NC). In this structure, graphene acts as a robust and conductive platform for the anchoring of MnO nanoparticles and the outer N-doped carbon can further guarantee the structural integrity and conductivity of the composite. When evaluated as anode materials in lithium-ion batteries, the prepared MnO@rGO/NC composite with an optimized amount of MnO (58%) exhibits stable cycling performance and superior high rate capability, which delivers a reversible capacity as high as 989.8 mA h g^{-1} at 0.2 A g^{-1} after 130 cycles. The design and synthetic strategy presented in this work can be extended to other anode materials with large capacity, which endure large volume expansion and low conductivity during the charge–discharge processes.

Introduction

In order to obtain higher energy density of lithium-ion batteries to meet the needs of the upscale markets of consumer electrons and electric vehicles, large-capacity anode materials have been intensively exploited, such as transition metal oxides and silicon-based anode materials [1–7]. Typically, MnO is

considered as a promising anode material due to the relatively low conversion potential (0.4–0.5 V vs. Li/Li$^+$), high theoretical capacity (756 mA h g^{-1}), non-toxicity, low cost and abundant source [8–11]. However, like most of the other large-capacity anode materials, the practical application of the MnO anode is still hindered by several disadvantages, such as rapid capacity fading caused by drastic volume

---

Tao Bai and Haochen Zhou contributed equally to this work.

Address correspondence to E-mail: j-yang@csu.edu.cn

change, pulverization and aggregation during the repeated charge/discharge process, and unsatisfactory rate capability arising from low intrinsic conductivity [12–16].

Up till now, many efforts have been devoted to solve these problems. One of the effective strategies is constructing MnO with nanostructure to alleviate the volume change during charge/discharge process and reduce the diffusion length for lithium ion [17–19]. However, nanostructured materials tend to self-aggregation during the charge/discharge process due to their high surface energy, which results in rapid capacity fading of the electrode. In addition, the side reactions related to the formation of the solid electrolyte interphase (SEI) layer will decrease the initial coulombic efficiency because of the large surface area [20–22]. Another alternative strategy is to prepare MnO/C nanocomposites by combining MnO particles with carbonaceous materials to improve the conductivity and alleviate the stress caused by drastic volume change during charge/discharge process [23–25]. For example, Zhang et al. [26] prepared MnO nanoparticles encapsulated in a three-dimensional porous carbon framework (MnO@CF) as an anode material, which exhibits relatively high specific capacity of 939 mA h g^{-1} at 0.2 A g^{-1} over 200 cycles. Gao et al. [27] synthesized MnO/C nanocomposite material as an anode material, which delivers a high capacity of 952 mA h g^{-1} at 0.1 A g^{-1} after 100 cycles. Yu et al. [28] successfully loaded MnO nanoparticles within a spherical carbon matrix as an anode material, which exhibits a reversible specific capacity of 501 mA h g^{-1} after 300 cycles at 0.5 A g^{-1}. The structural stability of the above mentioned materials during continuous change/discharge cycles is significant to heighten the cycle stability. Recent studies show that graphene used as electronic conducting framework for MnO could enhance electrochemical properties due to its excellent electrical conductivity, structural flexibility and large surface area. For instance, Cao et al. [29] fabricated MnO/rGO hybrid, which exhibits a reversible capacity of 847 mA h g^{-1} at 0.15 A g^{-1} after 50 cycles. Srikanth et al. [30] reported exfoliated graphene oxide/MnO composite, which exhibits a reversible capacity of 784 mA h g^{-1} after 100 cycles at 0.075 A g^{-1}. However, MnO particles were anchored onto the surfaces of graphene in the above MnO/graphene hybrids. It is inevitable that MnO particles will fall off from graphene during charge/

discharge process, which will affect the electrochemical performances. Therefore, a rational design of MnO/graphene composites with stable structure after repeated cycles is significant to solve these problems.

In this work, we report a facile synthesis of N-doped carbon-encapsulated MnO@rGO composite (MnO@rGO/NC), in which high-electric-conductivity graphene nanosheets act as platform for the uniform decoration of MnO nanoparticles, and further encapsulated by N-doped carbon layer for further protection. In this way, uniformly distributed MnO nanoparticles are sandwiched between graphene nanosheet and N-doped carbon layer. The collaboration of graphene nanosheet and carbon layer is expected to guarantee the structural stability and good conductivity of the composite, avoid the detachment of MnO, prevent pulverization and aggregation of MnO and facilitate the lithium ions transport. As a consequence, the proposed MnO@rGO/NC may exhibit enhanced electrochemical properties in terms of high reversible capacity, excellent cycling performance when used as anode materials in lithium-ion batteries.

Experimental

Synthesis of reduced graphene oxide

Generally, graphite oxide was synthesized according to a modified Hummers method [2]. Then, the prepared graphite oxide was dispersed ultrasonically into pure water to form GO solution with a concentration of 1.0 mg mL^{-1}, and basic magnesium carbonate was added into another deionized water to form suspension with a concentration of 10 mg mL^{-1}. After that, 200 mL of GO solution was added into 200 mL of basic magnesium carbonate suspension under stirring for 6 h. The product was collected, rinsed and dried at 90 °C and then processed at 800 °C in N$_2$ for 2 h. At last, the black product was washing with HCl solution, and rGO was collected, rinsed and dried.

Synthesis of MnO@rGO/NC

0.1 g of the as-prepared rGO powder and Mn(CH$_3$COO)$_2$·4H$_2$O were dispersed ultrasonically into 150 mL ethylene glycol, and then, 1 mL of hydrazine

hydrate acted as precipitant was added in. This reaction was carried out at 110 °C for 6 h under stirring. After that, the product was collected, rinsed and then dispersed ultrasonically in 400 mL of deionized water. Then, 0.48 g of Tris (hydroxymethyl) aminomethane, 0.4 g of polyethylene polypropylene glycol (F127) and 0.4 g of dopamine hydrochloride were added in under stirring. After 12 h, the precipitate was collected, rinsed and dried at 90 °C. Finally, the precursor was heated at 700 °C under Ar/H$_2$ atmosphere (Ar:H$_2$ = 90%:10%, volume) for 2 h. The MnO@rGO/NC composites originated from 1.6, 1.2 and 0.8 of Mn(CH$_3$COO)$_2$·4H$_2$O were designated as MGNC1, MGNC2 and MGNC3, respectively. For comparison, rGO/NC (designated as GNC), MnO@rGO [designated as MG, the weight of Mn(CH$_3$COO)$_2$·4H$_2$O is 0.8 g] and the pure MnO were obtained without adding Mn(CH$_3$COO)$_2$·4H$_2$O, dopamine and carbonaceous materials, respectively, in which other experimental procedures were not change.

Material characterization

The phase, morphologies and microstructures, composition and surface compositions and electronic states of the as-prepared samples were investigated by X-ray diffraction (XRD, Rigaku-TTRIII), scanning electron microscope (SEM, JSM-6360) and transmission electron microscopy (TEM, JEM-2100F), thermogravimetric analysis (TGA, SDTQ600), X-ray photoelectron spectra (XPS, ThermoFisher-VG scientific) and Raman spectroscopy (labRAM Hr800), respectively.

Electrochemical measurement

The electrochemical measurements were taken by using 2025 coin-type cells. The as-prepared composites, polyvinylidene fluoride (PVDF) and conductive carbon black were mixed with a mass ratio of 8:1:1 and dispersed in N-methylpyrrolidinone (NMP) to form slurry, and then the slurry was uniformly coated on a copper foil and dried at 120 °C to obtain working electrodes. For the typical electrode, the mass loading of the as-prepared composites was ca. 1.1 mg cm^{-2}. The coin cells were assembled in a glovebox filled with Ar atmosphere. The electrolyte was a solution of 1 mol L^{-1} LiPF$_6$ in a mixture of dimethyl carbonate and ethylene carbonate (volume ratio = 1:1), the separators were polypropylene membranes from Celgard, and the counter-electrodes were pure lithium foils. Galvanostatic discharge/charge tests were tested at different current densities within the range of 3.0–0.01 V versus Li$^+$/Li on a LAND testing measurement system. Electrochemical impedance spectroscopy (EIS) experiments and cyclic voltammograms (CV) measurements were taken on an electrochemical workstation (PARSTAT MC). CV measurements were taken at a potential range of 3.0–0.01 V versus Li$^+$/Li with a scan rate of 0.2 mV s^{-1}, and EIS experiments were performed in the frequency window of 0.01–100,000 Hz.

Results and discussion

The overall synthetic procedure of MnO@rGO/NC composite is illustrated in Fig. 1. Firstly, rGO was prepared by annealing basic magnesium carbonate@GO at 800 °C. As shown in Fig. S1, GO could attach to the surfaces of basic magnesium carbonate under stirring, and the presence of basic magnesium carbonate could solve the agglomeration of GO during the process of drying. After that, the precursor of MnO grew on the rGO and uniformly dispersed across the whole plane of rGO, leading to a uniform single MnO grain layer. In addition, polydopamine was in situ coating on the surface of the precursor. The MnO@rGO/NC composite was finally obtained by annealing in H$_2$/Ar atmosphere.

As shown in Fig. 2 and Fig. S2, the crystallographic structures of as-prepared products were characterized by XRD. It can be seen that the dominant diffractions of MG can be ascribed to Mn$_3$O$_4$ (JCPSD No. 24-0734), and the other weak diffractions can be indexed to MnOOH (JCPSD No. 18-0804). All the peaks of the precursors of MGNC1, MGNC2 and MGNC3 are Mn$_3$O$_4$, indicating that MnOOH was converted to Mn$_3$O$_4$ during the process of coating polydopamine. All the peaks of pure MnO, MGNC1, MGNC2, MGNC3 and MG can be assigned to MnO (JCPSD No. 07-0230), and no impurity phase is found, which means that Mn$_3$O$_4$/MnOOH was reduced to MnO completely after annealing the precursors in Ar/H$_2$ mixing atmosphere at 700 °C. The five diffraction peaks of MnO centered at 34.9°, 40.5°, 58.7°, 70.2° and 73.8° can be indexed as (111), (200), (220), (311) and

Figure 1 Schematic illustration for the synthesis of MGNC.
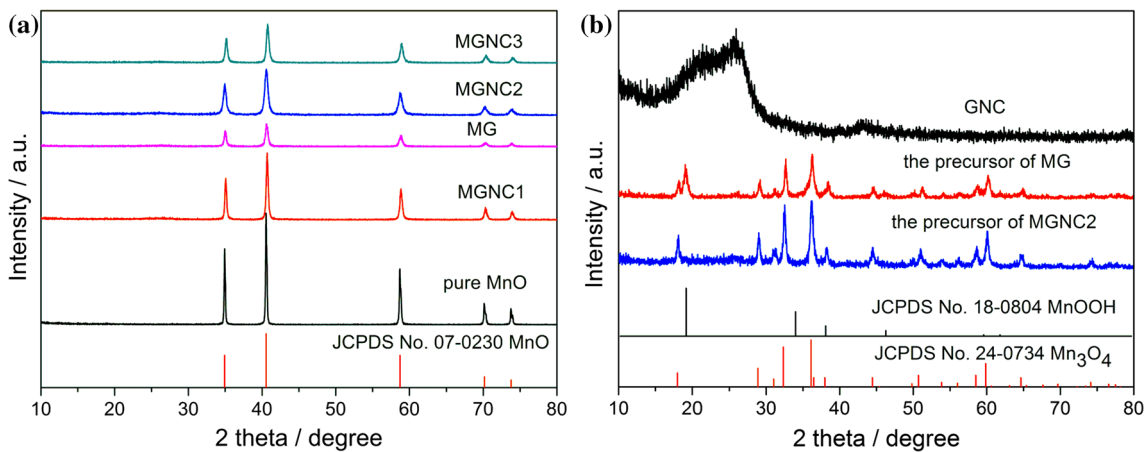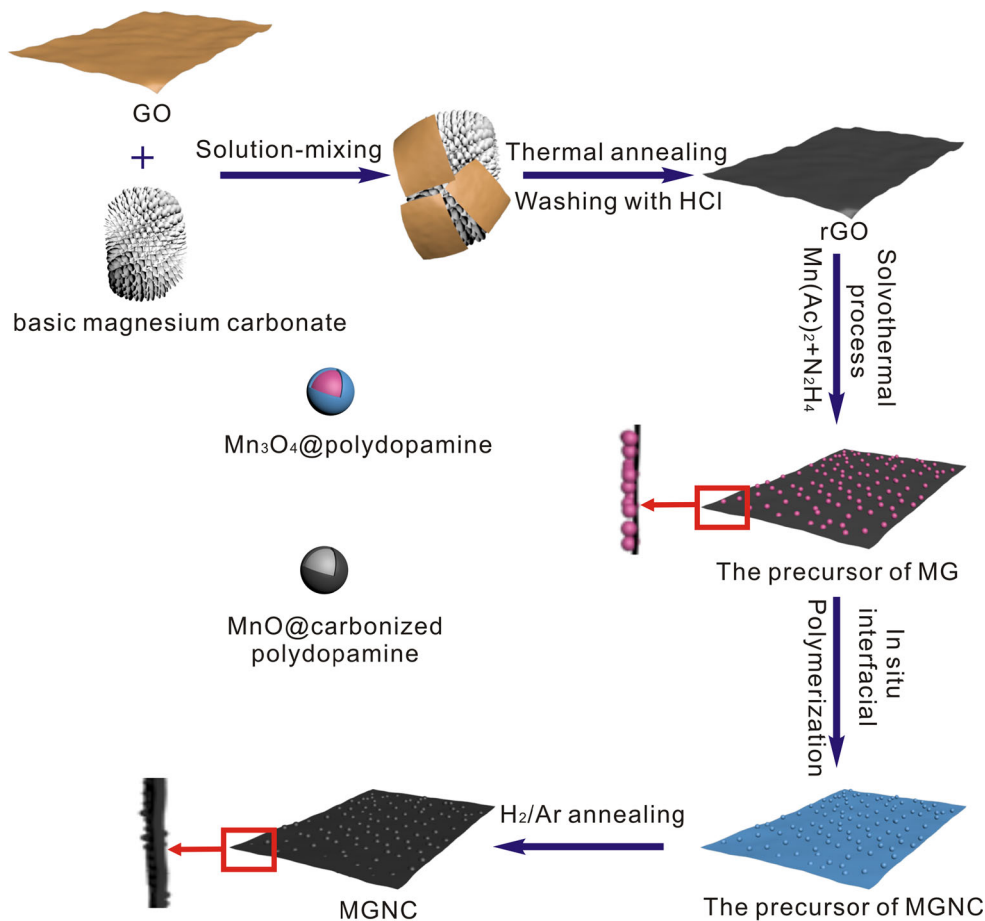
Figure 2 a XRD patterns of pure MnO, MGNC1, MG, MGNC2 and MGNC3. **b** XRD patterns of GNC, the precursor of MG and the precursor of MGNC2.

(222) lattice planes, respectively. As shown in Fig. 2b, GNC has a low graphitic degree according to the two broad peaks in XRD pattern, which is assigned to (002) and (100) lattice planes of carbon [31].

As presented in Fig. 3a, Raman spectra were obtained to further identify the structure of GNC, MGNC1, MGNC2, MGNC3 and MG. The broad peaks observed at ca. 1356 and 1593 cm^{-1} are
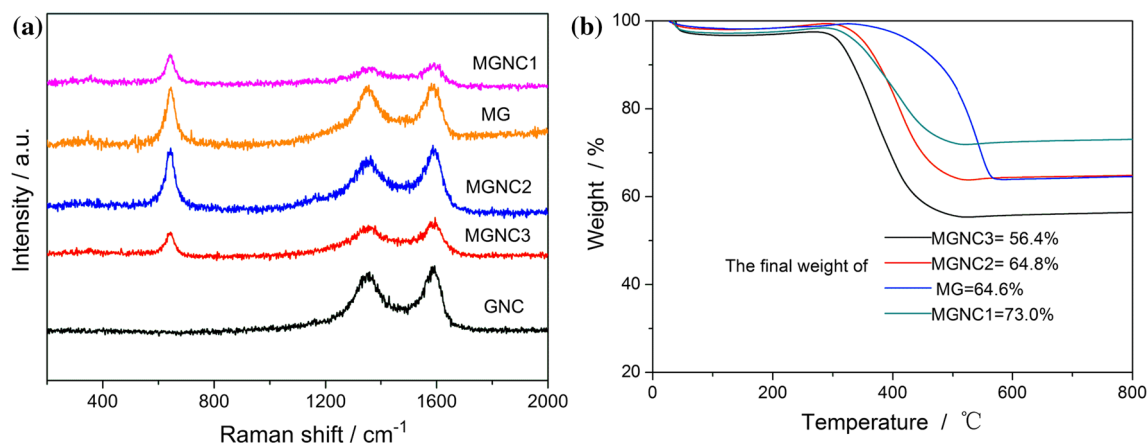
Figure 3 **a** Raman spectra of GNC, MGNC3, MGNC2, MG and MGNC1. **b** TGA curves of MGNC3, MGNC2, MG and MGNC1 (10 °C min^{-1} heating in air).

corresponding to the disordered band (D carbon) and graphitic band (G carbon) of carbon materials [32, 33]. The I_D/I_G intensity ratios of GNC, MGNC1, MGNC2, MGNC3 and MG are ca. 0.95, 0.97, 0.92, 0.92 and 0.99, respectively, demonstrating that the graphitic degree of the carbon in those materials is similar and it is independent of the existence or the absence of MnO. Additionally, the peak at around 642 cm^{-1} for MGNC1, MGNC2, MGNC3 and MG is assigned to the Mn–O vibration mode [30]. As shown in Fig. 3b, TGA analysis was carried out in air, from room temperature to 800 °C at a heating rate of 10 °C min^{-1}. The first weight loss from room temperature to ca. 200 °C can be ascribed to the evaporation of water absorbed on the surface of samples. The weight increased slightly in the temperature range from ca. 200 °C to ca. 310 °C, which was attributed to the oxidization of MnO in air. Afterward, the integrative effect of combustion of carbon and oxidation of MnO leads to a dramatic weight loss. The carbonaceous materials were entirely oxidized after ca. 600 °C, and manganese exists as Mn_2O_3 at ca. 800 °C according to the previous reports [10, 11]. Based on the TGA curves, it can be calculated that the content of MnO in MGNC1, MGNC2, MGNC3 and MG are 65.6, 58.3, 50.7 and 58.1%, and the content of carbon in MGNC1, MGNC2, MGNC3 and MG are 31.9, 40, 46.2 and 40.2%, respectively.

XPS analysis was carried out to investigate the surface compositions and electronic states of the as-prepared composites. The survey XPS spectra of MGNC2, MG and GNC are shown in Fig. 4a, the peaks of Mn 2p and O 1s are generated from MnO, and the peaks of C 1s, N 1s and O 1s are generated from rGO and nitrogen-doped carbon [8, 34]. As shown in Fig. 4b–d, the high-resolution XPS spectra of MGNC2 were investigated. The high-resolution C 1s peak (Fig. 4b) could be fitted into three parts centered at ca. 284.5, 285.2 and 289.1 eV, which are corresponding to the sp^2–sp^2 C, N–sp^2 C and C–O bonds. The high-resolution N 1s peak in Fig. 4c could be fitted into three parts centered at ca. 398, 400.4 and 403.7 eV, which are arising from pyridinic N, pyrrolic N and graphitic N bonds, respectively. Similarly, the high-resolution O 1s peak (Fig. 4d) could be fitted into two peaks centered at ca. 529.7 and 532.2 eV, which are indexed as Mn–O and C–O [35–37]. The high-resolution C 1s and N 1s spectra of GNC and the high-resolution C 1s spectrum of MG are shown in Fig. S3a–S3c, and these spectra are similar to the spectra of MGNC2. Thus, combining MnO with carbonaceous materials (rGO and nitrogen-doped carbon) has no effect on the composition of carbonaceous materials. As shown in the high-resolution Mn 2p spectra (Fig. S3d), two peaks at ca. 653.3 and 641.5 eV ascribed to Mn $2p_{1/2}$ and Mn$2p_{3/2}$ can be observed, which correspond to that of MnO [9].

The morphologies and microstructures features of the prepared composites were investigated by SEM and TEM. It can be seen from Figs. 5a and 6a that the size of pure MnO particles is ca. 70 × 200 nm^2 and these nanoparticles connect with each other
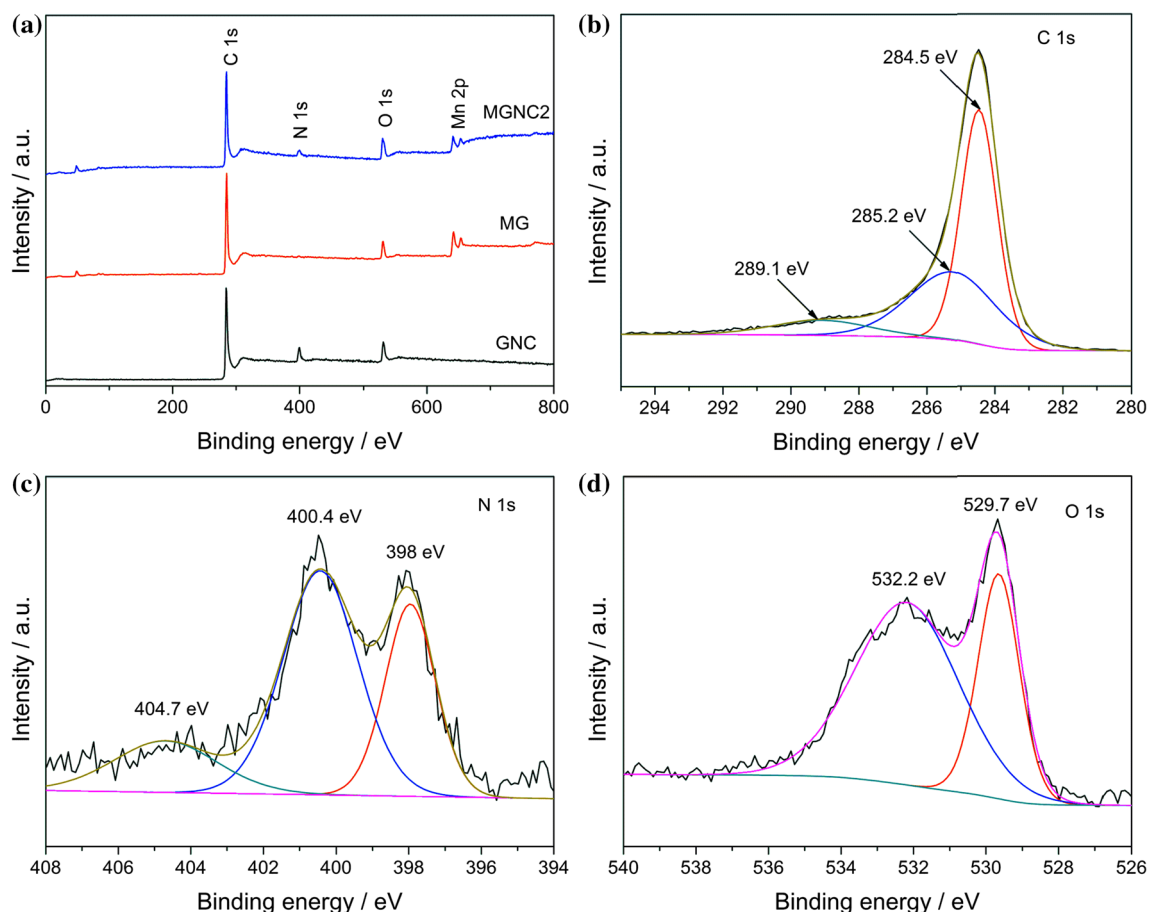
Figure 4 **a** Survey XPS spectra of MGNC2, MG and GNC. High-resolution XPS spectra of MGNC2: **b** C 1*s*, **c** N 1*s*, **d** O 1*s*.

randomly. As shown in Fig. S4a, basic magnesium carbonate consists of interconnected thick sheets with rough surfaces, which acted as hard template for preparing rGO. The morphology of rGO is shown in Fig. 5b and S5a. The size of rGO approximates with basic magnesium carbonate, indicating that basic magnesium carbonate is suitable for preventing the agglomeration of GO. Meanwhile, particular crumple morphology of two-dimensional structure in rGO could effectively act as supporting material for MnO nanoparticles. As shown in Figs. 5c and 6b, MnO particles were uniformly anchored on the thin layers of rGO. The size of MnO particles in MG is smaller than that of pure MnO. This is probably due to that crumple morphology in rGO could provide active point for the nucleation of MnO nanoparticles and restrict these particles growth. Figure 6c, d shows that the surface of MnO nanoparticles in MGNC2 is

coated by a thin carbon sheet, indicating that poly-dopamine was well coated on the surface of Mn_3O_4. It is demonstrated that single MnO grain layer was protected with graphene and nitrogen-doped carbon. From Fig. S4b to Fig. S4d, the surface becomes grainy obviously, indicating that the amount of MnO nanoparticles under nitrogen-doped carbon is increasing, and this is consistent with the content of MnO in these composites. As shown in Fig. 6d, the lattice distance of 0.221 and 0.255 nm in the HRTEM image of MGNC2 can be indexed as the (2 0 0) and (1 1 1) plan of MnO, respectively, and there is a thin carbon sheet outside of MnO corresponding to the nitrogen-doped carbon [19].

Figure 7a shows typical cyclic voltammetry curves of MGNC2 for initial three cycles. There are two reduction peaks at ca. 0.68 and 0.17 V in the first cycle, which is corresponding to the formation of SEI
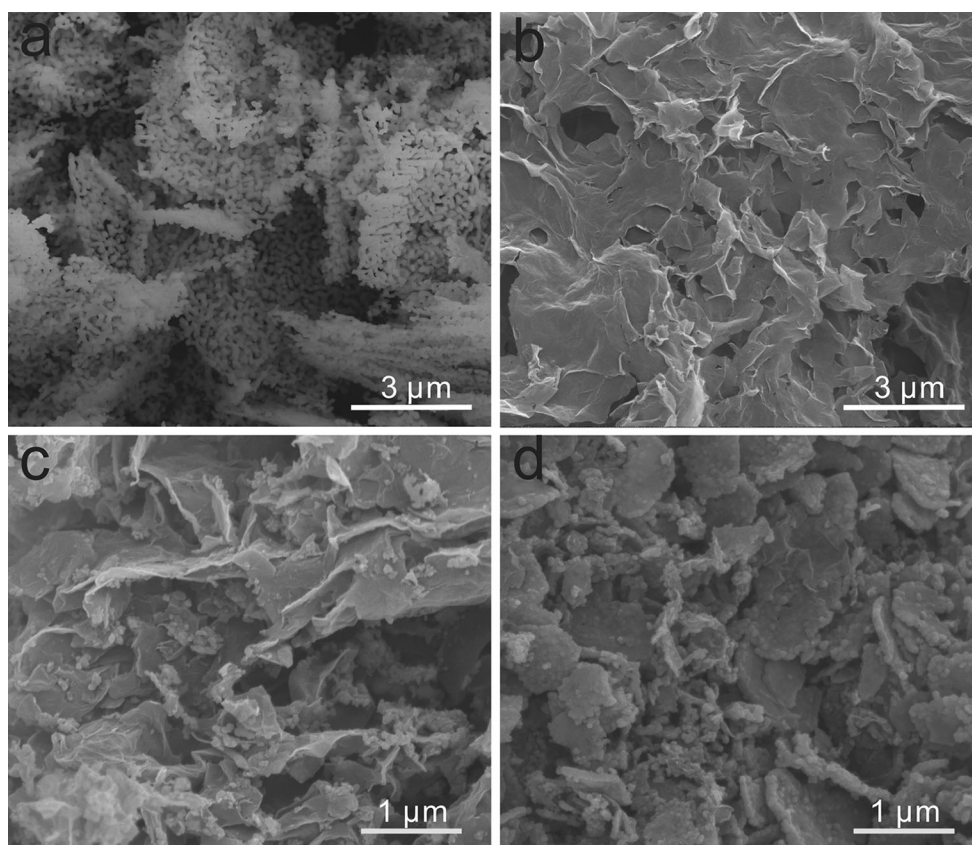
Figure 5 SEM images of **a** pure MnO, **b** rGO, **c** MG and **d** MGNC2.

layer and the reduction of Mn^{2+} to Mn^0, respectively. The peak at ca. 0.17 V shifts to ca. 0.4 V from the second cycle, which could be ascribed to the structure reconstruction induced by the formation of Li_2O and Mn [31, 38]. Meanwhile, there are two oxidation peaks at ca. 1.35 and 2.1 V, which are corresponding to the oxidation of Mn^0 to Mn^{2+} and the decomposition of the polymer/gel layer at above 2.0 V or the oxidizing of Mn^{2+} to a higher oxidation state [19, 26]. The MnO conversion reaction can be described as follows: $MnO + 2Li^+ + 2e^- \leftrightarrow Mn + Li_2O$ [39, 40]. Figure 7b shows the discharge/charge profiles of MGNC2 in the 1st, 2nd, 50th, 100th and 130th cycle at 0.2 A g^{-1}, and the plateaus in 1st and 2nd cycles match well with the peaks in the above CV curves. In the first cycle, there is a slope at ca. 0.9–0.6 V corresponding to the formation of SEI layer, which leads to an irreversible capacity, and the discharge and charge capacities are 1219.1 and 790.8 mA h g^{-1}, respectively. In the 50th, 100th and 130th discharge/charge

curves, a slope at ca. 1.8–2.1 V appears in the charge curves and another slope at ca. 0.7–1.3 V appears in the discharge curves, indicating that the Mn^{2+} in MGNC2 is oxidized to a higher oxidation state upon cycling and the conversion reaction is reversible. The main reason for this phenomenon can be ascribed to the fact that the conversion reaction kinetics was improved, because MnO particles were broken into ultrafine nanoparticles during charge/discharge process [22, 29].

As shown in Fig. 7c, the cycling performance of as-prepared materials was investigated at 0.2 A g^{-1}. After 130 cycles, the capacity of pure MnO, GNC, MG, MGNC1, MGNC2 and MGNC3 are 79.6, 389.7, 820.3, 316.5, 989.8 and 776.8 mA h g^{-1}, respectively. Among these MnO@rGO/NC composites, MGNC2 shows the best cycle performance, demonstrating that the MnO content in MGNC2 is the most suitable. The capacity of MGNC2 is still as high as 989.8 mA h g^{-1} after 130 cycles, which is higher
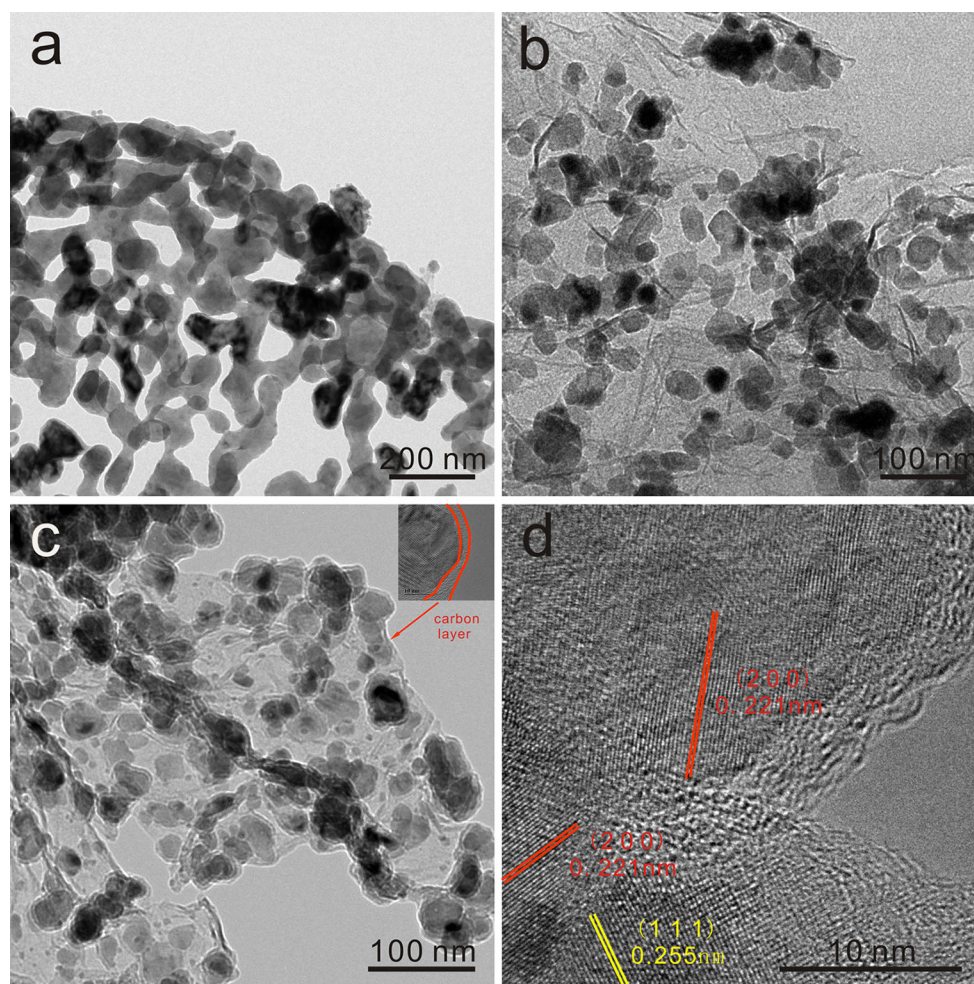
Figure 6 TEM images of **a** pure MnO, **b** MG, **c** MGNC2 and **d** HRTEM image of MGNC2.

than the theoretical capacity of MnO (756 mA h g^{-1}) based on the conversion reaction and the capacity of carbonaceous materials. As shown in Table S1, the electrochemical performance of MGNC2 is superior among those of the reported manganese oxide-based materials. It is noteworthy that the capacity of these MnO/C hybrids first drops and then increases upon cycling. The mechanism behind the capacity retention may be attributed to the decomposition of the polymer/gel layer during charge/discharge process, the oxidation of Mn^{2+} to a higher oxidation state during conversion process and the formation of N-doping defects [2, 8, 35, 38]. It can be seen from Fig. S6a that the coulombic efficiency of MGNC2 steadily increases to ca. 98% after several cycles, and MG has the lowest coulombic efficiency among these MnO/C hybrids, because of the absence of

nitrogen-doped carbon, the drastic volume change of MnO will break the structural integrity and destroy the as-formed SEI film, which results in increasing side reactions [22]. The results of TEM and HRTEM (Fig. 8) show that small MnO nanoparticles in MGNC2 are still coated by a thin carbon sheet after 200 cycles at 0.5 A g^{-1}, while MnO nanoparticles in MG break into smaller pieces with a diameter of ca. 2–3 nm and distribute in carbonaceous materials. It is inevitable that MnO nanoparticles in MG will fall off from carbonaceous materials and lose high conductivity benefited from graphene, which will deteriorate the electrochemical performances. These results are consistent with the electrochemical performances of these materials. As shown in Fig. S6b, MG and MGNC2 exhibit a reversible capacity of 383.9 and 712.7 mA h g^{-1} at
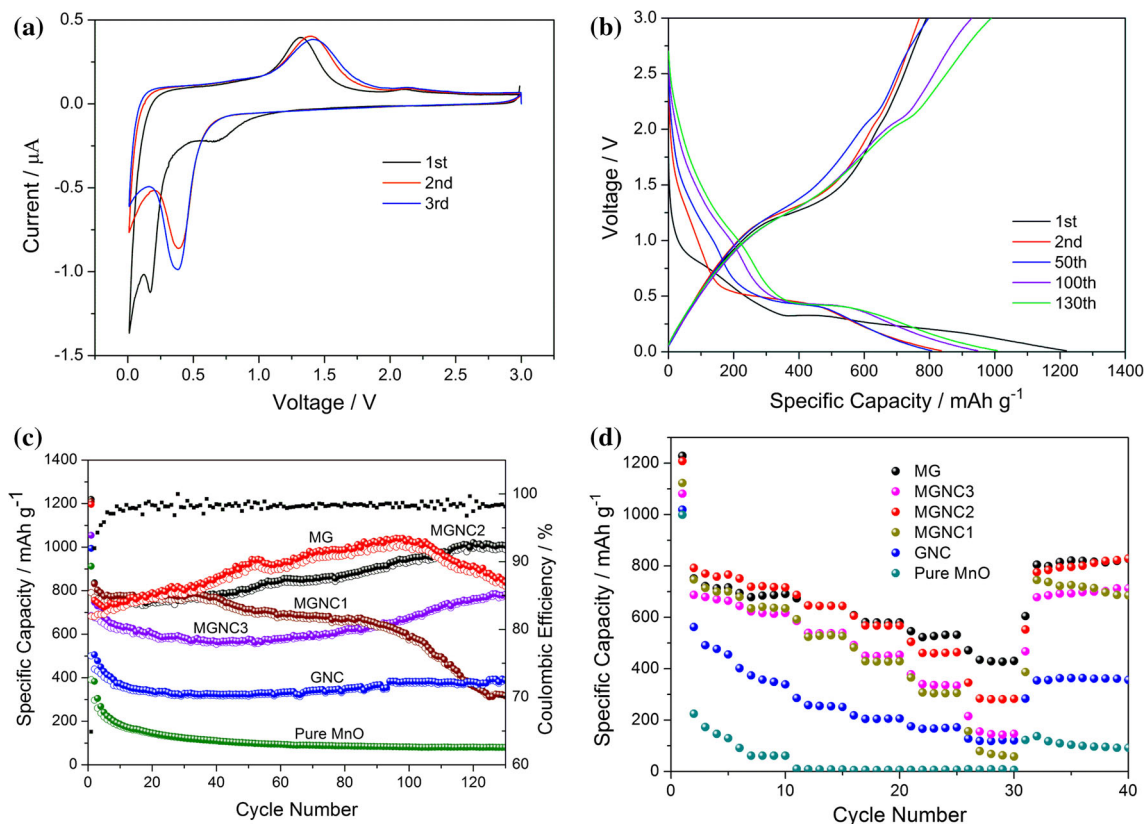
Figure 7 **a** Cyclic voltammogram curve of MGNC2 at a scan rate of 0.2 mV s^{-1}. **b** Discharge and charge profiles of MGNC2 at 0.2 A g^{-1}. **c** Cycles performances of pure MnO, GNC, MG, MGNC1, MGNC2 and MGNC3 at 0.2 A g^{-1}. **d** Rate performances of pure MnO, GNC, MG, MGNC1, MGNC2 and MGNC3 at various rates.

0.5 A g^{-1} after 200 cycles, respectively. Thus, the structure of MnO@rGO/NC is a rational design to improve the reliability and electrochemical properties for lithium-ion batteries.

The rate performances of the as-prepared materials were characterized at various current densities and are shown in Fig. 7d. For testing, the electrode was discharged and charged at same rate from 0.1 A g^{-1} to 5.0 A g^{-1} each for 5 cycles and then back to 0.1 A g^{-1} for 10 cycles. The reversible capacity of MG and MGNC2 is higher than that of GNC due to the existence of MnO. After combining with carbonaceous material, the rate performances of MG and MGNC2 are much better than that of pure MnO, indicating that carbonaceous material could efficiently buffer the volume change during conversion process and provide efficient electron transport pathways to improve the electrical conductivity. Meanwhile, the reversible capacity of MGNC2 is close to that of MG at low rate current densities, but

MGNC2 and MG deliver a reversible capacity of 281.3 and 421.8 mA h g^{-1} at 5 A g^{-1}. To gain further insight into the electron conductivity of the as-prepared composites, the electrochemical impedance spectra (EIS) of the as-prepared materials after activated for 3 cycles at 0.2 A g^{-1} were tested. As shown in Fig. S6c, a relevant equivalent circuit model is built up to fit the data points. R_o, R_s, R_{ct} and W_{o-} in this equivalent represent the bulk resistance of the cell attributed to the resistance of electrolyte, the SEI layer resistance, the charge-transfer resistance and the Warburg diffusion impedance ascribed to the diffusion of Li ions, respectively [13, 20]. R_{ct} of the pure MnO, MG, MGNC1, MGNC2 and MGNC3 and GNC electrodes are 165.6, 16.05, 47.17, 28.53, 26.44 and 14.89 Ω, respectively. It is consistent with the rate performances of these materials, which demonstrates that rGO which served as a conductive pathway could enhance the electron and Li-ions diffusion. Thus, carbonaceous material plays an important role
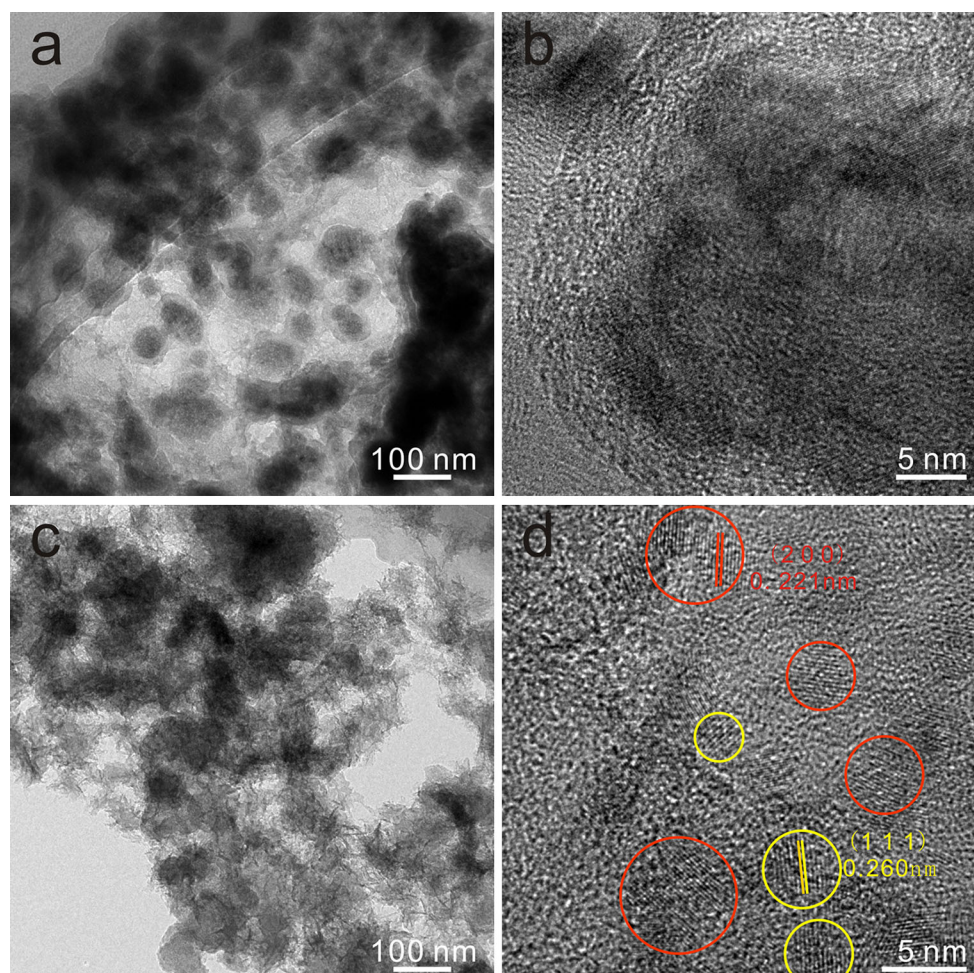
Figure 8 The anode materials after 200 cycles at 0.5 A g^{-1}: **a** TEM and **b** HRTEM images of MGNC2, **c** TEM and **d** HRTEM images of MG.

for the excellent reversible capacity and wonderful rate capability.

Conclusion

In summary, MnO@rGO/NC composite was successively fabricated via a step-by-step strategy. The structure is beneficial to the electron and Li-ions diffusion, graphene is used as electronic conducting framework and a volume buffer due to its excellent electrical conductivity and structural flexibility, and nitrogen-doped carbon coating layer is used to reinforce MnO nanoparticles on graphene. Owing to the rational design of the structure, MGNC2 with 58.3% MnO content exhibits a high reversible capacity of 989.8 mA h g^{-1} after 130 cycles at 0.2 A g^{-1}, even higher than theoretical value of MnO (756 mA h g^{-1}) based on the conversion reaction. Besides, the

integrity maintenance of MnO@rGO/NC composite during continuous change/discharge cycles is satisfactory, which is suitable for sufficient electrochemical reactions. Moreover, it is believed that the proposed rational design of structures can improve the reliability and electrochemical properties of other nanomaterials for lithium-ion batteries.

Acknowledgements

Electronic supplementary material: The online version of this article (doi:10.1007/s10853-017-1247-7)

contains supplementary material, which is available to authorized users.

References

[1] Etacheri V, Marom R, Elazari R, Salitra G, Aurbach D (2011) Challenges in the development of advanced Li-ion batteries: a review. Energy Environ Sci 4:3243–3262

[2] Zhang K, Han P, Gu L et al (2012) Synthesis of nitrogen-doped MnO/graphene nanosheets hybrid material for lithium ion batteries. ACS Appl Mater Interfaces 4:658–664

[3] Nam I, Kim ND, Kim G-P, Park J, Yi J (2013) One step preparation of Mn_3O_4/graphene composites for use as an anode in Li ion batteries. J Power Sources 244:56–62

[4] Dong S, Chen X, Gu L et al (2011) One dimensional MnO_2/titanium nitride nanotube coaxial arrays for high performance electrochemical capacitive energy storage. Energy Environ Sci 4:3502–3508

[5] Xu G, Zhang L, Guo C et al (2012) Manganese monoxide/titanium nitride composite as high performance anode material for rechargeable Li-ion batteries. Electrochim Acta 85:345–351

[6] Fu L, Zhang C, Chen B et al (2017) Graphene boosted Cu_2GeS_3 for advanced lithium-ion batteries. Inorg Chem Front 4:541–546

[7] Fu L, Wang X, Ma J et al (2017) Graphene-encapsulated copper tin sulfide submicron spheres as high-capacity binder-free anode for lithium-ion batteries. Chemelectrochem 4:1–7

[8] Sun Y, Hu X, Luo W, Huang Y (2012) Porous carbon-modified MnO disks prepared by a microwave-polyol process and their superior lithium-ion storage properties. J Mater Chem 22:19190–19195

[9] Luo W, Hu X, Sun Y, Huang Y (2013) Controlled synthesis of mesoporous MnO/C networks by microwave irradiation and their enhanced lithium-storage properties. ACS Appl Mater Interfaces 5:1997–2003

[10] Xu GL, Xu YF, Fang JC et al (2013) Facile synthesis of hierarchical micro/nanostructured MnO material and its excellent lithium storage property and high performance as anode in a MnO/LiNi0.5Mn1.5O(4-delta) lithium ion battery. ACS Appl Mater Interfaces 5:6316–6323

[11] Lee SM, Choi SH, Lee J-K, Kang YC (2014) Electrochemical properties of graphene-MnO composite and hollow-structured MnO powders prepared by a simple one-pot spray pyrolysis process. Electrochim Acta 132:441–447

[12] Sun Y, Hu X, Luo W, Xia F, Huang Y (2013) Reconstruction of conformal nanoscale MnO on graphene as a high-capacity and long-life anode material for lithium ion batteries. Adv Func Mater 23:2436–2444

[13] Huang SZ, Jin J, Cai Y et al (2014) Engineering single crystalline Mn3O4 nano-octahedra with exposed highly active 011 facets for high performance lithium ion batteries. Nanoscale 6:6819–6827

[14] Lee R-C, Lin Y-P, Weng Y-T, Pan H-A, Lee J-F, Wu N-L (2014) Synthesis of high-performance MnOx/carbon composite as lithium-ion battery anode by a facile co-precipitation method: effects of oxygen stoichiometry and carbon morphology. J Power Sources 253:373–380

[15] Liu B, Hu X, Xu H, Luo W, Sun Y, Huang Y (2014) Encapsulation of MnO nanocrystals in electrospun carbon nanofibers as high-performance anode materials for lithium-ion batteries. Sci Rep 4:4229

[16] Wang J-G, Jin D, Liu H et al (2016) All-manganese-based Li-ion batteries with high rate capability and ultralong cycle life. Nano Energy 22:524–532

[17] Jian G, Xu Y, Lai L-C, Wang C, Zachariah MR (2014) Mn_3O_4 hollow spheres for lithium-ion batteries with high rate and capacity. J Mater Chem A 2:4627–4632

[18] Su K, Wang C, Nie H, Guan Y, Liu F, Chen J (2014) Facile template-free synthesis of 3D porous MnO/C microspheres with controllable pore size for high-performance lithium-ion battery anodes. J Mater Chem A 2:10000–10006

[19] Xiao Y, Wang X, Wang W, Zhao D, Cao M (2014) Engineering hybrid between MnO and N-doped carbon to achieve exceptionally high capacity for lithium-ion battery anode. ACS Appl Mater Interfaces 6:2051–2058

[20] Wang S, Xiao C, Xing Y, Xu H, Zhang S (2015) Formation of a stable carbon framework in a MnO yolk–shell sphere to achieve exceptional performance for a Li-ion battery anode. J Mater Chem A 3:15591–15597

[21] Zhao G, Huang X, Wang X et al (2015) Synthesis and lithium-storage properties of MnO/reduced graphene oxide composites derived from graphene oxide plus the transformation of Mn(vi) to Mn(ii) by the reducing power of graphene oxide. J Mater Chem A 3:297–303

[22] Wang S, Xing Y, Xiao C, Xu H, Zhang S (2016) A peapod-inspired MnO@C core-shell design for lithium ion batteries. J Power Sources 307:11–16

[23] Liu H, Li Z, Liang Y, Fu R, Wu D (2015) Facile synthesis of MnO multi-core@nitrogen-doped carbon shell nanoparticles for high performance lithium-ion battery anodes. Carbon 84:419–425

[24] Jiang H, Hu Y, Guo S, Yan C, Lee PS, Li C (2014) Rational design of MnO/Carbon nanopeapods with internal void space for high-rate and long-life Li-ion batteries. ACS Nano 8:6038–6046

[25] Yuan T, Jiang Y, Sun W et al (2016) Ever-increasing pseudocapacitance in RGO–MnO–RGO sandwich nanostructures for ultrahigh-rate lithium storage. Adv Func Mater 26:2198–2206

[26] Wang S, Xing Y, Xu H, Zhang S (2014) MnO nanoparticles interdispersed in 3D porous carbon framework for high performance lithium-ion batteries. ACS Appl Mater Interfaces 6:12713–12718

[27] Yang C, Gao Q, Tian W et al (2014) Superlow load of nanosized MnO on a porous carbon matrix from wood fibre with superior lithium ion storage performance. J Mater Chem A 2:19975–19982

[28] Hu H, Cheng H, Liu Z, Yu Y (2015) Facile synthesis of carbon spheres with uniformly dispersed MnO nanoparticles for lithium ion battery anode. Electrochim Acta 152:44–52

[29] Jiang X, Zhu X, Liu X et al (2016) Nanospherical-like manganese monoxide/reduced graphene oxide composite synthesized by electron beam radiation as anode material for high-performance lithium-ion batteries. Electrochim Acta 196:431–439

[30] Petnikota S, Srikanth VVSS, Nithyadharseni P, Reddy MV, Adams S, Chowdari BVR (2015) Sustainable graphenothermal reduction chemistry to obtain MnO nanonetwork supported exfoliated graphene oxide composite and its electrochemical characteristics. ACS Sustain Chem Eng 3:3205–3213

[31] Wang J, Liu W, Chen J, Wang H, Liu S, Chen S (2016) Biotemplated MnO/C microtubes from spirogyra with improved electrochemical performance for lithium-ion batterys. Electrochim Acta 188:210–217

[32] Kang D, Liu Q, Si R, Gu J, Zhang W, Zhang D (2016) Crosslinking-derived MnO/carbon hybrid with ultrasmall nanoparticles for increasing lithium storage capacity during cycling. Carbon 99:138–147

[33] Guo J, Liu Q, Wang C, Zachariah MR (2012) Interdispersed amorphous MnOx-carbon nanocomposites with superior electrochemical performance as lithium-storage material. Adv Func Mater 22:803–811

[34] Liu J, Chen N, Pan Q (2015) Embedding MnO nanoparticles in robust carbon microsheets for excellent lithium storage properties. J Power Sources 299:265–272

[35] Gu X, Yue J, Chen L et al (2015) Coaxial MnO/N-doped carbon nanorods for advanced lithium-ion battery anodes. J Mater Chem A 3:1037–1041

[36] Sun Q, Wang Z, Zhang Z et al (2016) Rational design of graphene-reinforced MnO nanowires with enhanced electrochemical performance for Li-ion batteries. ACS Appl Mater Interfaces 8:6303–6308

[37] Chen W-M, Qie L, Shen Y et al (2013) Superior lithium storage performance in nanoscaled MnO promoted by N-doped carbon webs. Nano Energy 2:412–418

[38] Zhang Y, Chen P, Gao X et al (2016) Nitrogen-doped graphene ribbon assembled core-sheath MnO@graphene scrolls as hierarchically ordered 3D porous electrodes for fast and durable lithium storage. Adv Func Mater 26:7754–7765

[39] Zhang C, Wang J-G, Jin D, Xie K, Wei B (2015) Facile fabrication of MnO/C core–shell nanowires as an advanced anode material for lithium-ion batteries. Electrochim Acta 180:990–997

[40] Tang X, Sui G, Cai Q, Zhong W, Yang X (2016) Novel MnO/carbon composite anode material with multi-modal pore structure for high performance lithium-ion batteries. J Mater Chem A 4:2082–2088